Influence of nematic range on birefringence, heat capacity and elastic modulus near a nematic−smectic-*A* phase transition

F. Beaubois, T. Claverie, J. P. Marcerou, J. C. Rouillon, and H. T. Nguyen

Centre de Recherches Paul Pascal, Avenue Dr. Schweitzer, F-33600 Pessac, France

C. W. Garland and H. Haga*

Department of Chemistry and Center for Materials Science and Engineering, Massachusetts Institute of Technology, Cambridge, Massachusetts 02139

The birefringence Δn, the specific heat C_p, and the layer compressional elastic modulus **B** are reported for two liquid crystals near the nematic (N) to smectic-*A* (Sm*A*) phase transition. As predicted long ago by MacMillan and de Gennes [P. G. de Gennes and J. Prost, *The Physics of Liquid Crystals* (Clarendon, Oxford, 1993)] the coupling of the nematic orientational order parameter to the smectic-*A* layering order parameter can substantially alter the critical behavior near the N-Sm*A* transition if the nematic range is small and the nematic order parameter susceptibility is large. In this paper, we present a direct experimental comparison of two compounds: 4-octyloxy-4′-cyanobiphenyl (8OCB) with a short nematic range and 4-octyloxybenzoyloxy-4′-cyanotolane (C$_8$tolane) with a very large N range. The temperature variations of the apparent birefringence Δn and the specific heat C_p across the N-Sm*A* phase transition show the definite influence of the proximity of the isotropic phase in the case of 8OCB while the C$_8$tolane behaves as expected for the three-dimensional XY universality class. The elastic modulus **B** in the Sm*A* phase, measured at several wave vectors by the second-sound resonance technique, was studied with high resolution as a function of temperature on approaching $T_c(N$-Sm*A$)$. These elastic data confirm the **B** leveling off in both cases with an apparent breakdown of hydrodynamics in the case of the C$_8$tolane compound. [S1063-651X(97)02111-9]

PACS number(s): 64.70.Md, 65.20.+w, 62.20.Dc

I. INTRODUCTION

Liquid crystals have attracted interest from two points of view: applications and phase transitions. On the one hand, they respond easily to a weak electric constraint allowing the design of low consumption flat displays; on the other hand, they were thought to be rather versatile model systems for the study of phase transitions due to the almost infinite number of molecular structures accessible via organic synthesis. de Gennes soon realized that there were strong analogies between phase transitions in liquid crystals and more classical systems [1,2]. He first proposed that the nematic to smectic-*A* phase transition belonged to the three-dimensional (3D)-*XY* universality class like the condensation of superfluid helium with a two-component order parameter (modulus and phase of a complex number) defined in a three-dimensional space. He further showed that the analogy was closer to the normal to superconductor transition with the role of the vector potential **A** played by the director field **n**. At that time, it was hoped that the universality classes in phase transitions could be easily tested with liquid crystals, since the determination of the associated sets of critical exponents would be accessible by rather straightforward experimental techniques. Unfortunately, the situation is much

more involved, even for the rather simple nematic to smectic-*A* phase transition. Most of these complications are due to the anisotropy of the phases; for example, one has to define two correlation lengths $\xi_\parallel$ parallel to the director **n** and $\xi_\perp$ normal to it and two different associated critical exponents $\nu_\parallel$ and $\nu_\perp$. Another peculiarity comes from the strong coupling of smectic-*A* and nematic orders: the smectic-*A* layers are normal to the local director **n(r)** which direction has strong thermal fluctuations about its average. So it has been proposed that, when these fluctuations can be integrated out, the N-Sm*A* phase transition would always be first order, even if no latent heat was measurable [3]. It is well known also that the director would prefer a helicoidal precession in chiral compounds. This leads in the framework of the superconductor analogy already mentioned, to the existence in chiral systems of twist grain boundary phases that are analogous to Abrikosov's vortex lattices in superconductors [4]. In this paper, we are concerned with another smectic-nematic coupling involving the moduli of the respective order parameters.

II. MACMILLAN−de GENNES COUPLING

The smectic-*A* order parameter ψ can be written in the form of a plane wave of density modulation $|\psi| \exp[iq_s \mathbf{n} \cdot \mathbf{r}]$, where q_s is the wave vector of the layers, while the nematic order parameter Q_{ij} is a rank-2 traceless tensor with **n** as one eigenvector and up to two moduli Q and

*Permanent address: Department of Physics, Hokkaido University, Sapporo, Japan.

P if biaxial ($S \propto 3Q/2$ and $P=0$ if uniaxial),

$$Q_{ij} = \begin{pmatrix} -\dfrac{P+Q}{2} & 0 & 0 \\[2mm] 0 & \dfrac{P-Q}{2} & 0 \\[2mm] 0 & 0 & Q \end{pmatrix}. \quad (1)$$

MacMillan and de Gennes introduced in the nematic phase a coupling between the smectic order parameter ψ and the increment δS of the uniaxial nematic order parameter S which is already condensed [1,2],

$$\Delta F = \frac{1}{2\chi}\,\delta S^2 - C|\psi|^2\,\delta S, \quad (2)$$

where the susceptibility $\chi(T)$ is large near the nematic-isotropic transition point T_{NI} but smaller and smaller as one cools down deep into the nematic phase. When the free energy ΔF is minimized with respect to S, one recovers an increment in the nematic order parameter proportional to the square of the smectic density modulation,

$$\delta S_0 = \chi C|\psi|^2. \quad (3)$$

The effect of Eq. (3) is a renormalization of the quartic term of the smectic Landau free energy that may change the sign of the corresponding coefficient and drive the transition from second to first order via a tricritical point if the susceptibility χ is high enough, i.e., if the transition points T_{NI} and T_{NA} are close enough together.

Most of the earlier studies carried out at the N-SmA phase transition were done on compounds with short N ranges (typically a few kelvins). Thus the MacMillan–de Gennes coupling is often strong enough to put the critical phenomena under study in a crossover regime difficult to interpret. A typical example of such previously studied compounds is 4-octyloxy-4$'$-cyanobiphenyl $C_8H_{17}O\langle\varphi\rangle\langle\varphi\rangle CN$ (8OCB), where the symbol $\langle\varphi\rangle$ denotes a benzene ring. 8OCB belongs to the SmA_d class (partial bilayer) and has a short nematic range from 67 °C to 80 °C [5]. However, recent calorimetric studies of liquid crystals with large N ranges have shown that the excess heat capacity ΔC_p associated with the N-SmA phase transition conforms well to 3D-XY universality [6]. We have thus carried out a comparison of the N-SmA behavior of the birefringence Δn, the specific heat C_p, and the layer elastic constant **B** in 8OCB and in 4-octyloxybenzoyloxy-4$'$-cyanotolane (C$_8$tolane) with the structure $C_8H_{17}O\langle\varphi\rangle CO_2\langle\varphi\rangle\equiv C\langle\varphi\rangle CN$. The latter Sm$A_1$ compound (monolayer) is very stable, which allows for time consuming high resolution measurements, and exhibits a very large N range from 99 °C to $\sim$247 °C [7]. The new results for C$_8$tolane are compared with those for 8OCB, and it is shown that N-SmA coupling is not important for Δn and C_p in materials with a large nematic range whereas the behavior of **B** still shows an unexpected leveling off at the transition.
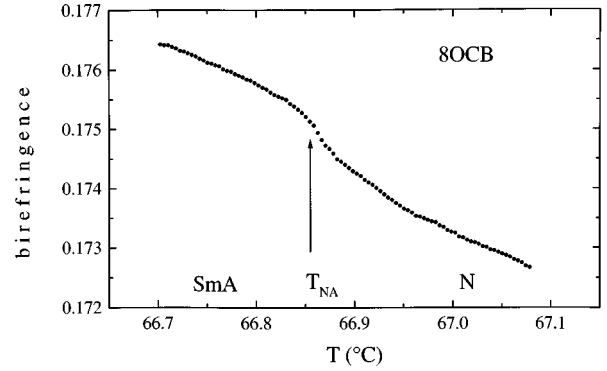

FIG. 1. Temperature behavior of the birefringence in 8OCB, showing the ordering induced by the onset of smectic layering.

III. BIREFRINGENCE MEASUREMENTS IN THIN CELLS

Contrary to what was stated in Ref. [8], where the data were influenced by a systematic error due to the swelling of the glue maintaining the cell plates, planar samples with a thickness in the micrometer range are uniaxial. Thus, we have measured the usual birefringence ($n_e - n_0$) between the extreme indices of refraction of a 2.6-μm-thick 8OCB sample and a 9.5 μm C$_8$tolane one. The birefringence is directly related to the nematic order parameter S (by means of the anisotropic part of the optical frequency dielectric tensor) by

$$n_e - n_0 = \frac{S\varepsilon_a}{2\langle n\rangle}, \quad (4)$$

where $\langle n\rangle^2 = (\varepsilon_\parallel + 2\varepsilon_\perp)/3$ and $\varepsilon_a = \varepsilon_\parallel - \varepsilon_\perp$, $\varepsilon_\parallel$ and $\varepsilon_\perp$ being the dielectric constants of a hypothetical perfectly aligned phase.

One can see in Fig. 1 for the case of 8OCB, where the nematic susceptibility χ is fairly large, a continuous
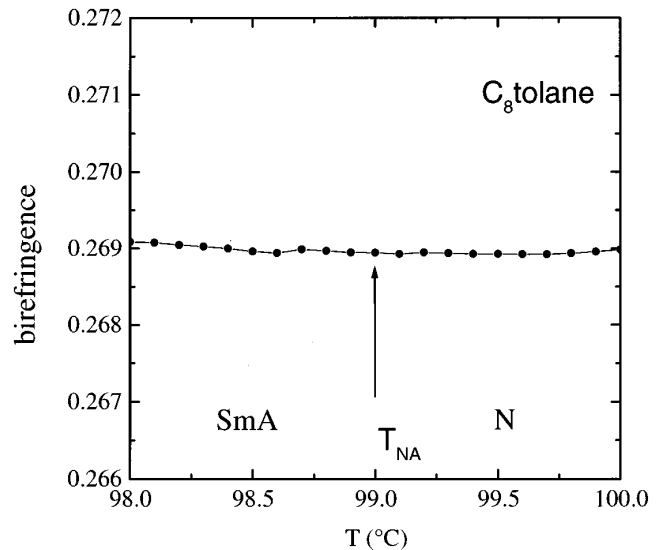

FIG. 2. The N-SmA phase transition has no visible influence on the birefringence of C$_8$tolane.

transition-induced increase in the birefringence $(n_e - n_0)$ occurs as soon as the fluctuations of ψ in the nematic phase become sizeable. On the contrary, in the case of C_8tolane as shown in Fig. 2, there is no obvious indication of any phase transition between nematic and smectic-*A* in the temperature dependence of the birefringence, which is perfectly smooth and quite flat near T_{NA}. One must remark that even with very high temperature resolution (a data point every 3 mK), the birefringence for 8OCB shows no apparent discontinuity in S at T_{NA} (driven by a discontinuity in $|\psi|^2$). This means that if the phase transition were to be first order in the sense of Halperin, Lubensky, and Ma [9] and Anisimov *et al.* [10], any discontinuity in the birefringence must be smaller than the experimental accuracy of about 3×10^{-5}. For C_8tolane, however, the susceptibility χ of the nematic order parameter is very low, since the nematic range is large and S is essentially saturated (the slope $d\Delta n/dt$ in the N phase is 7×10^{-3} for 8OCB but vanishingly small for C_8tolane). Thus, Eqs. (3) and (4) show that Δn for C_8tolane would not be sensitive to a discontinuous jump in $|\Psi|^2$, even it were to occur.

IV. HEAT CAPACITY RESULTS

The heat capacity $C_p(T)$ near the N-Sm*A* transition has been measured for a large variety of liquid crystals, including homolog series such as alkylcyanobiphenyl (*n*CB) as a function of chain length n and binary mixtures of homologs. The overall picture can be summarized as follows [6,11]. When the nematic range is large (and therefore the orientational susceptibility χ is small), the N-Sm*A* transition is second order with a C_p behavior that conforms to 3D-*XY* universality (critical exponent $\alpha_{XY} = -0.007$). As the nematic range is reduced, the transition remains second order but a crossover behavior is observed with the effective α varying from α_{XY} toward a tricritical value ($\alpha_t = 0.5$). For very short nematic ranges where χ is quite large, the nematic-smectic coupling can drive the coefficient of the $|\psi|^4$ term in the free energy negative, causing a first-order N-Sm*A* transition with a nonzero latent heat.

There is no calorimetric or x-ray evidence that coupling between Ψ and director fluctuations causes inverted *XY* behavior or detectable first-order character at the N-Sm*A* transition when the nematic range is moderate to large. Neither the early theory [9] suggesting such behavior nor the experimental dynamics of propagating interfaces [10], that is claimed to support first-order N-Sm*A* transitions, are definitive. Indeed, the dynamic experiments have all been carried out on systems with narrow N ranges that are close to the de Gennes tricritical point due to the Ψ-S coupling. The most recent high-resolution experiments and theory indicate normal (non-inverted) *XY* second-order behavior for systems with large N range except for some correlation length exponent anisotropy due to Ψ-δn coupling [6].

The compound 8OCB, which has been studied extensively [5,12], has a nematic range of 13.1 K and lies in the middle of the crossover regime. The $C_p(T)$ variation for 8OCB is shown in Fig. 3, and it is best described by an effective exponent $\alpha = 0.20 \pm 0.05$ [5,6].

High-resolution specific heat measurements have been made with an ac calorimeter at MIT on samples of C_8tolane. The experimental techniques have been well described else-
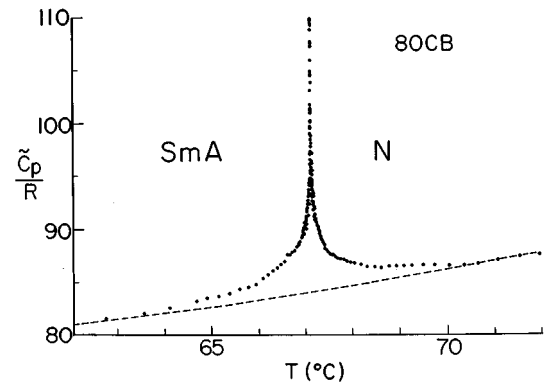

FIG. 3. Heat capacity of 8OCB in the vicinity of the N-Sm*A* transition (taken from Ref. [5b]). The quantity displayed is the dimensionless ratio of the molar heat capacity $\widetilde{C}_p$ to the gas constant R. Conversion to a specific heat in J K^{-1} g^{-1} units can be easily made using the molecular weight of 8OCB (307.44 g mol^{-1}). The dashed line represents $\widetilde{C}_p/R$ (background) for the N-Sm*A* region.

where [13] and will not been given here. The resulting C_p values are given in Fig. 4 at two frequencies (ω_0 and $\omega_0/3$, where $\omega_0 = 0.196$ s^{-1} corresponds to 31.25 mHz). The excellent agreement between the ω_0 and $\omega_0/3$ values shows that the experimental C_p corresponds to the static thermodynamic limit. Furthermore, C_p data for C_8tolane were very stable over a series of runs lasting two months: the T_c value drifted by only 25 mK and the shape and size of the $C_p(N$-Sm*A*) peak were unchanged. Characteristic changes in the phase shift between the ac heater input power and the T_{ac} oscillating sample temperature are a very sensitive qualitative indication of the presence of two coexisting phases, which must occur if a transition is first order [13]. No such phase shift anomalies were observed for C_8tolane.

The excess heat capacity ΔC_p associated with the N-Sm*A* transition was analyzed with the power-law form given by renormalization group theory and used previously to analyze other liquid crystal $\Delta C_p(N$-Sm*A*) data [6,14],
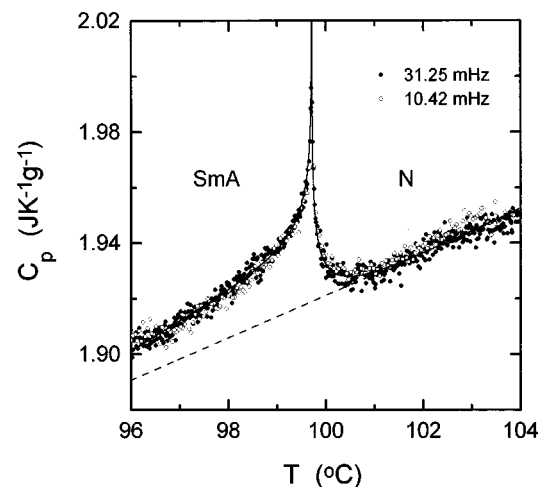

FIG. 4. Specific heat C_p for C_8tolane in the vicinity of the N-Sm*A* transition. The dashed line represents C_p (background). The solid line is fit 8 to ΔC_p with Eq. (5); see Table I for the least-squares-fitting values.

TABLE I. Least-squares values of the adjustable parameters for fitting $\Delta C_p(N\text{-}SmA)$ data of C_8tolane with Eq. (5). Quantities in brackets were held fixed at the given values. t_{min} values are 2.9×10^{-5} and -8.6×10^{-5}. The units of A^+, A^-, and B_c are JK^{-1} g^{-1}, and the estimated standard deviation for C_p data points is 0.0025 JK^{-1} g^{-1}.

Fit	$|t|_{max}$	α	T_c (K)	A^+	A^-/A^+	D_1^+	D_1^-/D_1^+	D_2^+	D_2^-/D_2^+	B_c	χ_v^2
1	0.003	-0.021	372.868	-1.075	0.974	-0.662	0.875	[0]	[1]	0.919	1.06
2	0.006	-0.020	372.872	-0.928	0.967	-0.513	0.670	[0]	[1]	0.804	1.02
3	0.010	-0.015	372.873	-1.119	0.972	-0.379	0.557	[0]	[1]	1.006	1.03
4	0.003	[-0.007]	372.868	-2.782	0.991	-0.244	0.884	[0]	[1]	2.642	1.06
5	0.006	[-0.007]	372.872	-2.319	0.988	-0.197	0.665	[0]	[1]	2.207	1.02
6	0.010	[-0.007]	372.873	-2.195	0.987	-0.194	0.544	[0]	[1]	2.090	1.03
7	0.006	[-0.007]	372.862	-3.428	0.995	-0.348	1.387	0.986	2.585	3.248	0.92
8	0.010	[-0.007]	372.868	-2.895	0.992	-0.303	1.005	0.666	1.731	2.746	0.99

$$\Delta C_p = A^{\pm}|t|^{-\alpha}(1+D_1^{\pm}|t|^{\Delta_1}+D_2^{\pm}|t|)+B_c, \qquad (5)$$

where $\Delta C_p = C_p(\text{observed}) - C_p(\text{background})$ and $C_p(\text{background})$ represents all the contributions to C_p that would be present even in the absence of the $N\text{-}SmA$ phase transition. The quantity t is the reduced temperature $(T-T_c)/T_c$, and Δ_1 is the corrections-to-scaling exponent. The background line shown in Fig. 4 and used in the fits is $C_p(\text{background}) = 1.919 + 0.0076(T-T_c)$. The asymmetric ΔC_p shape for C_8tolane is typical of liquid crystals with 3D-XY critical heat capacities [6(b),14]. A series of fits to the $\Delta C_p(\omega_0)$ data shown in Fig. 4 were made with Eq. (5), and the values of the least-squares fitting parameters are given in Table I. Fits 1–3 show the effects of range shrinking when α is taken to be a freely adjustable parameter and Δ_1 is held fixed at 0.5. These three fits are in good agreement, and the critical exponent α is quite stable at small negative values. Since the C_p data are compatible with $\alpha = \alpha_{XY}$, as expected for a liquid crystal with a very large nematic range [6,14], the remaining fits in Table I were obtained with α held fixed at the $\alpha_{XY} = -0.007$ value and Δ_1 fixed at the XY value 0.524. Note that when $\alpha < 0$, ΔC_p is a singular *cusp* with a finite value B_c as the maximum value at T_c and amplitudes $A^{\pm}$ that are negative. None of the numerous exploratory fits made initially to C_8tolane ΔC_p data showed systematic deviations or anomalous parameter values that would suggest first-order character (such as $\alpha^+ \neq \alpha^-$, $T_c^+ \neq T_c^-$ or $B_c^+ \neq B_c^-$).

The choice of XY exponents allows the C_8tolane experimental amplitude ratios to be compared with theory and with the fitting results for other XY-like liquid crystals. Previous analysis of $\Delta C_p(N\text{-}SmA)$ for XY-like systems has shown that second corrections-to-scaling terms usually play a significant role. Thus fits 4–6 were made with $D_2^{\pm} = 0$ and fits 7 and 8 with $D_2^{\pm}$ as free nonzero parameters. Although a good χ_v^2 value can also be obtained for a fit over the $|t|_{max} = 0.003$ range when $D_2^{\pm} \neq 0$, this fit is not given in Table I since the amplitude values are unreliable when this form is used over such a narrow range. The 3D-XY universal theoretical value of A^-/A^+ is 0.9714 ± 0.0126 [15], and several liquid crystals with large nematic ranges (96 K or larger) have experimental A^-/A^+ values in the range 0.986 -0.994 [6]. Thus for C_8tolane fits 6 and 8, the values $A^-/A^+ = 0.987\pm0.004$ and 0.992 ± 0.004 are in good agreement with previous work. One expects theoretically that

$D_1^-/D_1^+ = 1$, and the experimental results on XY-like liquid crystals range from 0.7 to 1.3 [6]. Again the C_8tolane fit 8 value $D_1^-/D_1^+ \simeq 1.00\pm0.35$ is consistent with expectations. Thus all the universal aspects of $\Delta C_p(N\text{-}SmA)$ are fully compatible with 3D-XY behavior. This conclusion is supported by the fact that power-law fits to another C_8tolane run with a greater density of data points but a smaller $|t|_{max}$ range of 0.006 gave essentially the same parameter behavior as shown in Table I.

Only seven liquid crystals had previously been known to exhibit $\Delta C_p(N\text{-}SmA)$ peaks that conform to 3D-XY theory [6(a)], and only five of those had been analyzed in great detail [6(b),14]. The C_p behavior of C_8tolane is quite similar to that of the compounds $T7$ and $T8$, where Tn is 4-alkyloxybenzoyloxy-4'-cyanostilbene. The structure of Tn compounds is very similar to that of $C_n$tolanes (Tn has a —CH=CH— bridging group in place of the —C≡C— group in $C_n$tolanes), and the T-vs-n phase diagrams are topologically the same for both homolog series. Thus, the present calorimetric study of C_8tolane provides another good demonstration that liquid crystals with very large nematic range have critical excess heat capacities ΔC_p that conform to 3D-XY universality. It should be kept in mind, however, that x-ray data show that these compounds still exhibit a small anisotropy of the smectic correlation lengths in the nematic phase ($\nu_\parallel > \nu_\perp$) due to coupling between the smectic order parameter and director fluctuations [6(a)].

V. CRITICAL BEHAVIOR OF THE ELASTIC MODULUS B

Having characterized the substantial influence of the nematic range on two properties of the studied compounds, let us examine the sensitivity of the layer compressional elastic modulus **B** in the smectic phase to the same parameter. We first have to recall the present status of the **B** problem, i.e., its behavior when approaching the nematic phase in case of a second-order phase transition.

In the mean-field approximation, **B** is simply proportional to the square of the modulus of the smectic-A order parameter, $|\psi|^2$, thus vanishing with a critical exponent $2\beta = 1$. Such a behavior has never been observed experimentally, confirming that fluctuations do play a role at this transition as seen from other techniques.

Then it was shown [1,2] that **B** should behave like the

inverse correlation length ξ^{-1}; hence, for the 3D-*XY* universality class, it should vanish with the critical exponent $\nu_{XY} = 0.67$. If the nematic range is small enough, the MacMillan–de Gennes coupling would lead the transition to exhibit crossover behavior toward a tricritical point where fluctuations are Gaussian. In the limiting case of tricriticality, the quantities $|\psi|^2$ and ξ^{-1} approach zero in the same manner (with tricritical exponents $\nu_t = 2\beta_t = 0.5$) and **B** should vanish as $|t|^{0.5}$. Thus one would expect a crossover behavior from 3D-*XY* to tricritical. Unfortunately, power-law fits with $\mathbf{B} \sim |t|^{\varphi}$ yield effective critical exponents φ that are usually in the range 0.3 to 0.4 [16], which is outside the 0.5 to 0.67 expected range.

The next step has been to take into account the already mentioned anisotropy of the correlation lengths and their exponents, which leads to a more refined prediction that **B** should vary like $\xi_\parallel / \xi_\perp^2 \propto |t|^{2\nu\perp - \nu\parallel}$ [17]. This leads to a much greater freedom for the numerical values of the empirical **B** critical exponent φ. One expects that φ should equal $(2\nu_\perp - \nu_\parallel)$ and be consistent with the x-ray determined values of $\nu_\parallel$ and $\nu_\perp$ in the nematic phase: for example, in 8OCB [18], $\nu_\parallel \simeq 0.67 \pm 0.03$ and $\nu_\perp \simeq 0.51 \pm 0.04$, which would yield $\varphi = 0.35 \pm 0.11$; the published empirical results $0.29 \leqslant \varphi \leqslant 0.49$ agree fairly well with this x-ray range [16,19].

A theoretical treatment of the anisotropic *N*-Sm*A* model led to only two stable fixed points [20]: namely, an inverted 3D-*XY* one (i.e., an inverted ratio of the excess specific heats amplitudes, so A^-/A^+ is larger than 1) with $\nu_\parallel = \nu_\perp = 0.67$, and a highly anisotropic one with $\nu_\parallel = 2\nu_\perp$. The first fixed point has already been discussed, and it should be noted that an inverted A^-/A^+ ratio has never been verified experimentally; but the second fixed point raises interesting questions especially when dealing with the **B** modulus. It implies a $|t|^0$ law, i.e., a nonvanishing of **B** at the transition. More precisely, as first stated by Nelson and Toner [21], **B** should decrease with power laws terms arising from corrections-to-scaling down to a nonzero value B_0 at T_c,

$$B = B_0 + B_1 |t|^{\varphi_1} + B_2 |t|^{\varphi_2}. \tag{6}$$

It has been reported for the first time by Fish, Sorensen, and Pershan [22] in 6OCB-8OCB mixtures, that the elastic modulus **B** measured with the help of second-sound resonance was nonvanishing at the *N*-Sm*A* phase transition. Some of the present authors [23] have confirmed this result in various compounds with rather small nematic ranges, fitting the **B**(*T*) data with only a first order corrections-to-scaling term yielding $B_0 \approx 10^7$ dyn cm^{-2} and $\varphi_1 = \Delta_1 \approx 0.5$.

Nevertheless, as for the inverted 3D-*XY* point, all the experimental determinations of $\nu_\parallel$ and $\nu_\perp$ disagree with the extreme anisotropy $\nu_\parallel = 2\nu_\perp$, as discussed in reference [6]. The present work addresses several different aspects of the apparent nonvanishing of **B** at the transition. First of all, as we have seen previously, there may be a strong influence of a narrow nematic range on the studied compounds and this might lead to an apparent **B** leveling off in some materials. Thus, a comparative study of 8OCB and C$_8$tolane is of value. The coupling of director fluctuations and the smectic order parameter, which is the cause of anisotropy in ν values, should not play a role in a compound like C$_8$tolane where the *N* range is very large [6]. Second, the nonvanishing of **B** at

T_c has been attributed recently [24] to the fact that the frequency of the propagating second-sound wave becomes too high compared to the critical slowing down of the characteristic frequency of the smectic order parameter, so that the experiments were not done in the hydrodynamic regime close to the transition. This would lead to a measured quantity **B** that is apparently temperature independent near T_{NA} i.e., nonvanishing. We present in the Appendix the way we have addressed this problem, following closely a demonstration due to Lubensky [25]. Third, we compare fits of Eq. (6) to **B**(|*t*|) data with and without a finite B_0 value (i.e., with and without the constraint $\nu_\parallel = 2\nu_\perp$).

Reported below are the experimental **B**(*T*) results for both compounds 8OCB and C$_8$tolane. As stated above, two types of fit have been carried out. For the first kind, one assumes a nonvanishing ($B_0 > 0$) and expects in the Nelson-Toner limit a first correction exponent φ_1 (to be compared to the calorimetric one $\Delta_1 \approx 0.5$) and if necessary φ_2 (compared to $2\Delta_1 \approx 1$). Conversely, we tried fits with $B_0 = 0$ where in order to be coherent with x-ray data, one expects $\varphi_1 = 2\nu_\perp - \nu_\parallel$ and $\varphi_2 = \varphi_1 + 0.5$.

A. The second sound resonance technique

The experimental technique has been extensively described elsewhere [26]. Let us just mention that an electric field, which is periodic in the direction of the layers ($q_x = 157$ cm^{-1}) and in time with a frequency ranging from 1 to 200 kHz, is applied to a 1-mm-thick homeotropic sample. Let us be aware that one cannot measure **B** over a wide range of wavevectors (or frequencies) with total confidence. At low enough frequencies, dislocations can move to relax stresses, which results in an apparent reduction of **B** [27]. At frequencies above a few MHz, relaxation processes often set in, leading to an apparent increase in **B**. Second sound resonances give access to a frequency window well below typical nonhydrodynamic relaxation frequencies and well above those characteristic of dislocation motion [28]. When scanning the frequency, one excites successive resonances of a compression-undulation stationary wave, the so-called second sound. Since there exists a trivial q dependence due to dispersion relations, let us extract the elastic modulus **B** which is not q dependent in the hydrodynamic regime,

$$\rho \omega_r^2 = B \frac{q_x^2 q_n^2}{q_x^2 + q_n^2} = B \frac{q_x^2(n^2\pi^2/4D^2)}{q_x^2 + (n^2\pi^2/4D^2)}, \tag{7}$$

where ρ is the density ≈ 1 g cm^{-3} and $q_x^2 = 2.5 \times 10^4$ cm^{-2} is linked to the period of the applied electric field. Using Eq. (7), one computes a series of data for the values of an apparent **B**(*T*) that will reveal (or not) a hydrodynamic behavior if they are (or not) independent of wave vector and frequency at a given temperature *T*. The transition temperature T_{NA} is determined by up to three different methods (i) the disappearance of resonances in Sm*A* phase, (ii) the vanishing of a low frequency signal in *N* phase on cooling down, and (iii) the annealing of typical smectic defects) [29].

B. Experimental results for 8OCB

The bare temperature dependence of the resonance frequencies $\omega_r/2\pi$ at wave vectors $n\pi/2D$ is shown in Fig. 5 for 8OCB (*D* is the sample thickness of 1 mm and $n = 1, 3,$ or 5).
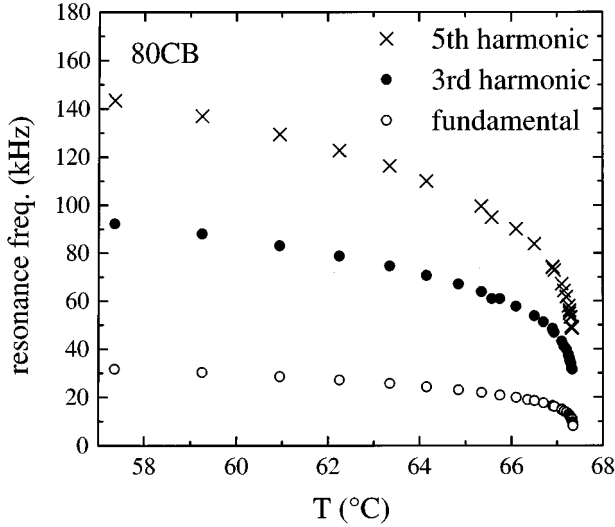
FIG. 5. Temperature variation of the second-sound resonance frequencies for the fundamental wave vector $\pi/2D$ and the harmonics $3\pi/2D$ and $5\pi/2D$ for 8OCB.

One readily sees that the resonance frequencies are decreasing when approaching the transition; conversely, the characteristic time of the smectic-A order parameter fluctuations increases following the law $\tau \sim \xi^z \sim |t|^{-zv}$ (z is the dynamic exponent defined in the Appendix). If it happens that the product $\omega_r \tau$ crosses over from <1 far from T_{NA} to >1 near it, the hydrodynamic regime would be lost and ω_r would become temperature independent but still wave-vector-q dependent. One can plot $\mathbf{B}$ as a function of reduced temperature $|t| = |T_{NA} - T|/T_{NA}$ as in Fig. 6. One then sees that the three different determinations of $\mathbf{B}$ are superimposable on the same curve proving that the final leveling off is not due to the loss of the hydrodynamic regime. The loss of third and fifth harmonics for $|t| < 10^{-4}$ is due to the damping of resonances that did not allow a reliable fit.

Several different fits are reported in Table II. Fit 1 is the nonvanishing one with Tc fixed at the average of measured values (methods i and ii of section V A). The $\mathbf{B}_0$ and φ_1 ($=\Delta_1$) values are coherent with previously reported ones [23] and with Nelson-Toner expectations for the corrections-to-scaling. The χ_v^2 value of 1.19 reflects systematic devia-
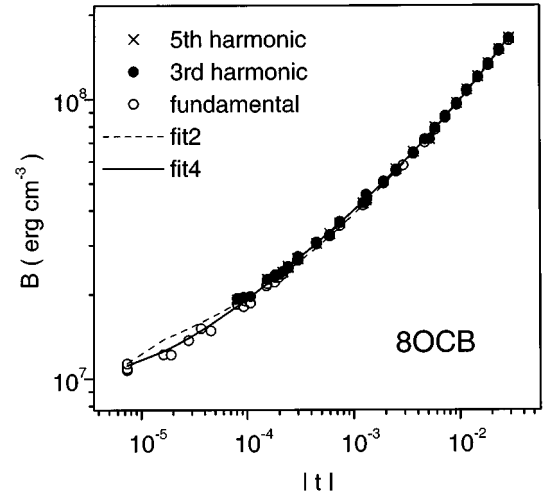

FIG. 6. Log-log plot of the $\mathbf{B}$ values of 8OCB calculated from Eq. (7) for three different harmonics. The solid and dashed lines represent fits 2 and 4 in Table II.

tions for $|t| < 10^{-4}$ that may (artificially or not) be suppressed by letting T_c be an adjustable parameter (decreasing in order to improve χ_v^2). The resulting parameters are given as fit 2.

Fits 3 and 4 show variations of the second kind ($B_0 = 0$) each with a constraint. For fit 3, T_c is fixed and one gets the best χ_v^2 of 0.8 but $\varphi_1 = 0.167 \pm 0.02$ and $\varphi_2 = 0.587 \pm 0.02$ do not agree well with the expectations $(2\nu_\perp - \nu_\parallel) = 0.35 \pm 0.11$ and $\varphi_2 = \varphi_1 + 0.5$. If T_c is allowed to be an adjustable free parameter, the resulting fit is the same as fit 3. In the case of fit 4 where $\varphi_2 = \varphi_1 + 0.5$ is required, the exponent $\varphi_1 = 0.291$ agrees reasonably well with $2\nu_\perp - \nu_\parallel$ although χ_v^2 is slightly higher and the effective T_c is 4 mK above the measured one.

In summary, second-sound propagation at different wavevectors in 8OCB is found to be in a hydrodynamic regime, yielding a $B(|t|)$ behavior that can be reasonably fitted with a Nelson-Toner law ($B_0 \neq 0$, fit 1) or with a power law ($B_0 = 0$, $\varphi = 0.29$, fit 4) after the introduction in both cases of a first-order corrections-to-scaling term $|t|^{0.5}$. This last result is reminiscent of previously published results on the same compound [30–32] where an exponent φ of about 0.3 was

TABLE II. Least-squares values of the adjustable parameters for fitting $B(|t|)$ data in 8OCB and the third harmonic of second-sound resonance in C_8tolane. $|t_{min}|$ values computed from measured T_c are 7.3×10^{-6} for 8OCB and 8×10^{-6} for C_8tolane. The units of B_i coefficients are erg cm^{-3}, and the estimated standard deviation for B data points is 10^6 erg cm^{-3} for 8OCB and 4×10^6 erg cm^{-3} for C_8tolane.

| Data set	Fit	T_c (K)	$10^{-7} B_0$	φ_1	$10^{-8} B_1$	φ_2	$10^{-10} B_2$	χ_v^2
8OCB	1	[340.495]	1.070	0.501	8.991		[0]	1.19
8OCB	2	340.493	1.132	0.510	9.302		[0]	1.13
8OCB	3	[340.495]	[0]	0.167	0.704	0.587	0.100	0.80
8OCB	4	340.499	[0]	0.291	2.605	[$\varphi_1 + 0.5$]	0.118	1.06
C_8tolane	5	[372.209]	1.911	0.706	81.03		[0]	1.33
C_8tolane	6	[372.209]	0.461	0.351	5.672	0.868	1.15	1.00
C_8tolane	7	[372.209]	[0]	0.277	3.31	0.838	1.12	0.98
C_8tolane	8	372.213	[0]	0.337	5.69	0.88	1.19	0.98
C_8tolane	9	372.218	[0]	0.351	5.90	[$\varphi_1 + 0.5$]	1.07	1.03
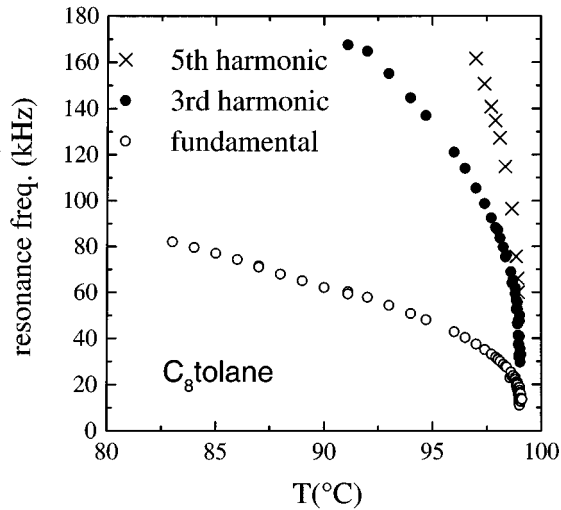
FIG. 7. Resonance frequencies of second-sound resonance harmonics in C_8tolane. The bare values are higher than for 8OCB due to the stiffer elasticity of SmA_1 compounds.

reported. This is not surprising if one recalls that these experiments dealing with B/K were made in a very narrow region close to the transition where no correction term was necessary.

C. Experimental results for C_8tolane

When measured under the same conditions as previously, C_8tolane yields the bare $\omega_r/2\pi$ data shown in Fig. 7. Note that the resonance frequencies increase much faster than for 8OCB due to the stiffer character of SmA_1 as compared to SmA_d.

The greater stiffness of SmA_1 materials is confirmed when one extracts the **B** values using Eq. (7). As shown in
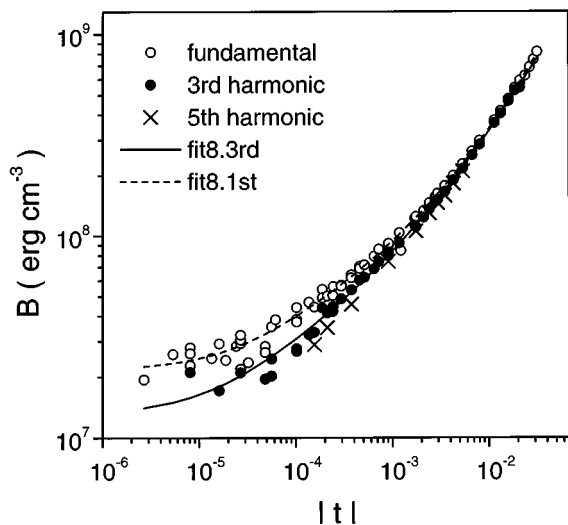

FIG. 8. Log-Log plot of the **B** values in C_8tolane for different harmonics. The first and third harmonics are not superimposable. The solid line represents fit 8 for the third harmonic in Table II, while the dashed one is the same fit done with the first harmonic's data.
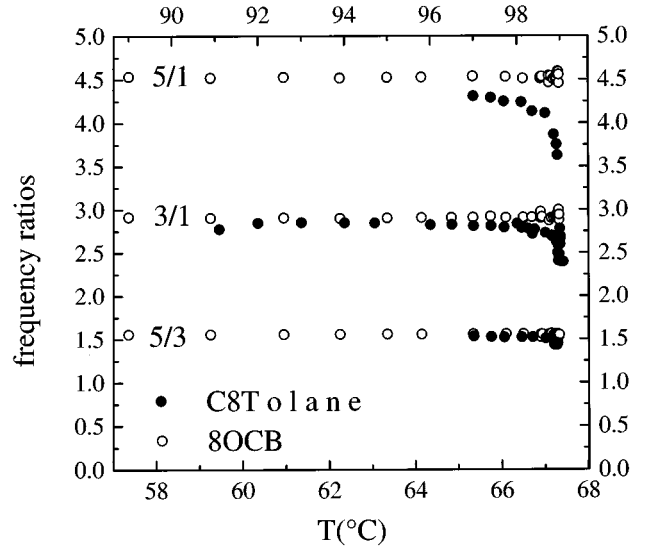

FIG. 9. Plot of the *ratios* of resonance frequencies. Top: 5th over 1st harmonic; middle: 3rd over 1st, and bottom: 5th over 3rd. It appears that 8OCB (open circles, left and bottom axes) obeys Eq. (7) with constant **B**, whereas C_8tolane (filled circles, right, and top axes) does not. This is the signature of hydrodynamic breakdown in C_8tolane as **B** cannot be considered to be wavevector independent.

Fig. 8, the elastic modulus **B** in the SmA_1 phase ~ 15 K below T_{NA} is of the order of 10^9 dyn cm^{-2}. More importantly, Fig. 8 shows that there is still a leveling off of the elastic modulus as T approaches T_{NA}. This implies that this effect is not due to the short N range of previously studied compounds. This answers one criticism.

Figure 8 shows also that the **B** values are slightly larger when determined from the second-sound first harmonic than from the third and fifth harmonics. This cannot be due to a crossover from $\omega_r\tau<1$ to $\omega_r\tau>1$, since one would have expected the reverse behavior, i.e. as shown in the appendix, the plateau values at the transition temperature would have been in the sequence $B_0(5\pi/2D)>B_0(3\pi/2D)>B_0(\pi/2D)$ if dynamic crossover had occurred. It could also be attributed, as suggested by Fig. 9, to an anomalous increase in the resonance frequency of the second-sound fundamental mode in the vicinity of the transition. This behavior is not usually observed since one may excite up to the 17th harmonic of the second-sound resonance [33] without noticing any discrepancy in the dispersion relation given in Eq. (7). A breakdown of hydrodynamics at vanishing frequencies and wave vectors has already been predicted [34] and verified by the second-sound technique [33], but this involves much smaller relative variations in **B** and leads to a decrease of few percent in the fundamental resonance frequency instead of the large *increase* observed here.

Despite the nonhydrodynamic behavior revealed by the first harmonic of the second-sound resonance, we made separate fits to first-harmonic and third-harmonic data sets. There were not a sufficient number of data points for the fifth harmonic to permit a fit to those data. The results obtained with the third harmonic, which we believe to be most reliable, are reported in Table II, and the results for the first harmonic were similar to the reported ones with comparable exponents but greater χ_ν^2 and B_i parameters. Fit 5 with nonvanishing B_0

and one power law gives $\varphi_1 = 0.706$ (0.739 for the first harmonic), which is not the expected first corrections-to-scaling exponent. Fits 6 and 7 hold T_c fixed but allow a nonzero $B_2 |t|^{\varphi_2}$ term. In the case of fit 6 (where B_0 is free) a very small B_0 value is obtained, and fit 7 (where $B_0 \equiv 0$) is of equal quality. The last two fits in Table II allow T_c to be an adjustable parameter. In fit 8, the χ_ν^2 does not improve but φ_1 increases to 0.337 (0.335 for the first harmonic) and φ_2 is close to $\varphi_1 + 0.5$, as shown by fit 9. The exponent $\varphi_1 = 0.35$ in fit 9 is quite similar to the 8OCB value $\varphi_1 = 0.29$ in fit 4, but this C_8tolane exponent is far away from the expectation $\varphi_1 = 2 \nu_\perp - \nu_\parallel \approx 0.56$ based on similar $T7$ and $T8$ compounds [6].

In summary, second-sound propagation at different wavevectors in C_8tolane reveals an unexpected and unusual breakdown of hydrodynamics. Fitting the $B(|t|)$ behavior of the third harmonic can be done with a Nelson-Toner law ($B_0 \neq 0$, but with a $|t|^{0.7}$ correction term, fit 5) or with a power law including corrections-to-scaling ($B_0 = 0$, $\varphi_1 \approx 0.35$, $\varphi_2 \approx 0.85$, fit 9).

No straightforward explanation can be given for our observations. It is, however, perhaps worth noting the already mentioned analogy between $C_n$tolane and Tn chemical compounds. Recall that the Tn series is famous for giving rise to a nematic reentrance (N-SmA_d-N_r-SmA_1) with its $T8$ member [35], which is also the case for C_9tolane [7]. So C_8tolane over its large N phase range may undergo significant changes in its short-range order from SmA_d-like to SmA_1-like [36] and this might explain the anomalous hydrodynamic behavior in smectic-A phase.

VI. SUMMARY

This comparative study of two compounds with very different nematic temperature ranges has confirmed that the coupling between nematic and smectic order is responsible for the birefringence increase and the crossover exponent of the excess specific heat for 8OCB at the N-SmA phase transition. It has also shown that C_8tolane near the N-SmA_1 transition does not show any anomaly in the birefringence and the critical behavior of the specific heat behaves as expected for the 3D-XY universality class.

On the contrary, the determination of the elastic modulus **B** by the second-sound resonance technique shows a leveling off just below $T_c(N$-Sm$A)$ for both compounds. This elastic result is not sensitive to the extent of the nematic range in contrast to the Δn and C_p results. This may be due to the fact that the second-sound technique involves a periodic excitation in the kHz range while the two other techniques are at zero or vanishing low frequencies. A simultaneous study at different wave vectors proves that 8OCB second-sound resonances are always in the hydrodynamic regime while C_8tolane shows an unusual wave-vector dependence.

APPENDIX: DYNAMICAL SCALING

In the second-sound resonance technique, one creates in a homeotropic smectic-A sample a stationary perturbation at a given wave vector and adjustable frequency. An optical setup sensitive to the light scattering by this periodic perturbation allows the determination of the response function of the layers (forgetting the intrinsic anisotropy),

$$\chi_u(\omega, q, T) \propto \frac{1}{Bq^2 - \rho \omega^2 + j \gamma \omega q^2}, \qquad \text{(A1)}$$

where B is the elastic modulus, ρ the density, and γ an effective viscosity. A resonance occurs each time the frequency ω_r matches the condition $Bq^2 \sim \rho \omega_r^2$, where one reaches a pole of the response function χ_u. Dynamical scaling tells us that $\chi_u(\omega, q, T)$ is a homogeneous function of $\omega^{1/z}$, q, and the reduced temperature $t = (T_{NA} - T)/T_{NA}$ via $\xi \sim |t|^{-\nu}$, where ν is the coherence length critical exponent and z is the dynamical scaling exponent such that the relaxation time τ for the order parameter goes like $\xi^z \sim |t|^{-z\nu}$:

$$\chi_u(\omega, q, T) \propto \chi_u^{\text{homo}}(\omega^{1/z}, q, \xi^{-1}) \propto \xi^y \chi_u^{\text{homo}}(\omega^{1/z}\xi, q\xi, 1). \qquad \text{(A2)}$$

The poles of the function χ_u are given by a unique function $\omega_r \xi^z (q\xi)$ which has two different scaling behaviors in the hydrodynamic ($\omega_r \tau \ll 1$, where $B \sim \omega_r^2/q^2$ depends only on t) and nonhydrodynamic ($\omega_r \tau \gg 1$, where $B \sim \omega_r^2/q^2$ depends only on q) regimes. In any case, $\omega_r \xi^z$ behaves like the power law $(q\xi)^x$ so that

$$\frac{B}{\rho} = \frac{\omega_r^2}{q^2} = \frac{\omega_r^2 \xi^{2z}}{q^2 \xi^2} \, \xi^{2-2z} \propto q^{2x-2} \xi^{2x-2z}. \qquad \text{(A3)}$$

In the hydrodynamic regime one has $x = 1$ so that $B \sim \xi^{2-2z}$, while in the nonhydrodynamic regime close to T_{NA} one should get $x = z$ so that $B \sim q^{2z-2}$. In the framework of the 3D-XY universality class, one may assume that $z = 3/2$, hence B crosses over from a ξ^{-1} law to a q^{+1} law. Experimentally, if the leveling off we observed near T_c were due to this crossover, it can be checked easily by selecting the wave vector q at different resonant harmonics $q = \pi/2D$, $3\pi/2D$, and $5\pi/2D$, where D is the sample thickness of about 1 mm. If a nonvanishing of **B** is observed which is more or less proportional to q, this will indicate nonhydrodynamic behavior.

[1] P. G. de Gennes and J. Prost, in *The Physics of Liquid Crystals* (Clarendon, Oxford, 1993).

[2] S. Chandrasekhar, in *Liquid Crystals* (Cambridge University Press, Cambridge, 1992).

[3] J. Thoen, H. Marynissen, and W. Van Dael, Phys. Rev. Lett. **52**, 204 (1984).

[4] S. R. Renn and T. C. Lubensky, Phys. Rev. A **38**, 2132 (1988).

[5] (a) C. W. Garland, G. B. Kasting, and K. J. Lushington, Phys.

Rev. Lett. **43**, 1420 (1979); G. B. Kasting, K. J. Lushington, and C. W. Garland, Phys. Rev. B **22**, 321 (1980); I. Hatta and N. Nokoyama, Mol. Cryst. Liq. Cryst. **66**, 417 (1981); J. M. Viner and C. C. Huang, Solid State Commun. **39**, 789 (1981). (b) R. J. Birgeneau, C. W. Garland, G. B. Kasting, and B. M. Ocko, Phys. Rev. A **24**, 2624 (1981).

[6] (a) C. W. Garland and G. Nounesis, Phys. Rev. E **49**, 2964 (1994) and references cited therein. (b) C. W. Garland, G. Nounesis, M. J. Young, and R. J. Birgeneau, Phys. Rev. E **47**, 1918 (1993).

[7] H. T. Nguyen and H. Gasparoux, Mol. Cryst. Liq. Cryst. Lett. **49**, 287 (1979).

[8] F. Beaubois and J. P. Marcerou, Europhys. Lett. **36**, 111 (1996).

[9] B. I. Halperin, T. C. Lubensky, and S. Ma, Phys. Rev. Lett. **32**, 292 (1974).

[10] M. A. Anisimov, P. E. Cladis, E. E. Godoretskii, D. A. Huse, V. E. Podneks, V. G. Taratuta, W. Van Saarloos, and V. P. Voronov, Phys. Rev. A **41**, 6749 (1990).

[11] J. Thoen, in *Phase Transitions in Liquid Crystals*, Vol. 290 of *NATO Advanced Study Institute, Series B: Physics*, edited by S. Martellucci and A. N. Chester (Plenum, New York, 1992), pp. 155–174 and references cited therein.

[12] J. D. Litster, J. Als-Nielsen, R. J. Birgeneau, S. S. Dana, D. Davidov, F. Garcia-Golding, M. Kaplan, C. R. Safinya, and R. Schaetzing, J. Phys. (Paris) **40**, C3-339 (1979).

[13] C. W. Garland, Thermochim. Acta **88**, 127 (1985); T. Chan, C. W. Garland, and H. T. Nguyen, Phys. Rev. E **52**, 5000 (1995); C. W. Garland, in *Liquid Crystals: Physical Properties and Phase Transitions*, edited by S. Kumar (Oxford University Press, Oxford, in press).

[14] C. W. Garland, G. Nounesis, and K. J. Stine, Phys. Rev. A **39**, 4919 (1989).

[15] C. Bervillier, Phys. Rev. B **34**, 8141 (1986).

[16] M. Benzekri, J. P. Marcerou, H. T. Nguyen, and J. C. Rouillon, Phys. Rev. B **41**, 9032 (1990).

[17] T. C. Lubensky and J. H. Chen, Phys. Rev. A **17**, 366 (1978).

[18] A. R. Kortan, H. Von Kanel, R. J. Birgeneau, and J. T. Litster, J. Phys. (France) **45**, 529 (1984).

[19] M. Benzekri, Ph.D. thesis, Université Bordeaux I, 1990 (unpublished).

[20] T. C. Lubensky, J. Chim. Phys. (France) **80**, 31 (1983).

[21] D. R. Nelson and J. Toner, Phys. Rev. B **24**, 363 (1981).

[22] M. R. Fish, L. B. Sorensen, and P. S. Pershan, Phys. Rev. Lett. **48**, 943 (1982).

[23] M. Benzekri, T. Claverie, J. P. Marcerou, and J. C. Rouillon, Phys. Rev. Lett. **68**, 2480 (1992).

[24] P. Martinoty, P. Sonntag, L. Benguigui, and D. Collin, Phys. Rev. Lett. **73**, 2079 (1994).

[25] T. Lubensky (private communication).

[26] J. Prost and P. S. Pershan, J. Appl. Phys. **47**, 2298 (1976).

[27] P. S. Pershan and J. Prost, J. Appl. Phys. **46**, 2343 (1975).

[28] L. Ricard and J. Prost, J. Phys. (Paris) **40**, C3-83 (1979).

[29] T. Claverie, Ph.D. thesis, Université Bordeaux I, 1994 (unpublished).

[30] N. A. Clark, Phys. Rev. A **14**, 1551 (1976).

[31] J. D. Litster, J. Als-Nielsen, R. J. Birgeneau, S. S. Dana, D. Davidov, F. Garcia Golding, M. Kaplan, C. R. Safinya, and R. Shaetzing, J. Phys. (Paris) **40**, C3-339 (1979).

[32] H. J. Fromm, J. Phys. (Paris) **48**, 647 (1987).

[33] J. C. Rouillon, M. Benzekri, T. Claverie, J. P. Marcerou, H. T. Nguyen, and J. Prost, Liq. Cryst. **16**, 1065 (1994).

[34] G. Grinstein and R. Pelcovits, Phys. Rev. Lett. **47**, 856 (1981).

[35] F. Hardouin, G. Sigaud, M. F. Achard, and H. Gasparoux, Solid State Commun. **30**, 265 (1979); H. T. Nguyen, A. Pourrère, and C. Destrade, *ibid.* **62**, 125 (1980).

[36] K. W. Evans-Lutterodt, J. W. Chang, B. M. Ocko, R. J. Birgeneau, C. Chiang, C. W. Garland, E. Chin, J. Goodby, and H. T. Nguyen, Phys. Rev. A **36**, 1387 (1987).